Molecular Crystals and Liquid Crystals
Publication details, including instructions for authors and subscription information:
http://www.tandfonline.com/loi/gmcl16

The Triplet State in Pyrene

K. Mistelberger [a] & H. Port [a]
[a] Physikalisches Institut, Teil 3, Universitaet Stuttgart, D 7000, Stuttgart 80, West Germany

Version of record first published: 14 Oct 2011.

To cite this article: K. Mistelberger & H. Port (1980): The Triplet State in Pyrene, Molecular Crystals and Liquid Crystals, 57:1, 203-226

To link to this article: http://dx.doi.org/10.1080/00268948008069827

Mol. Cryst. Liq. Cryst., 1980, Vol. 57, pp. 203–226
0026-8941/80/5701-0203$04.50/0

Printed in U.S.A.

The Triplet State in Pyrene

Optical manifestation of excitonic energy transfer in the dimeric high and low temperature crystalline phases

K. MISTELBERGER and H. PORT

Physikalisches Institut, Teil 3, Universitaet Stuttgart, D7000 Stuttgart 80, West Germany

Both emission and excitation spectra of phosphorescence and delayed fluorescence of pyrene single crystals have been investigated between 2 K and 300 K using cw dye laser excitation. The experiments prove that the lowest triplet state is excitonic in nature in the high and low temperature crystalline phases. No evidence for triplet excimer emission could be found. The so-called regular broad band triplet excimer emission was spectrally resolved at low temperature and identified as trap emission. On the basis of polarized high resolution excitation spectra of undoped normal and perdeuterated pyrene (supplemented by Zeeman spectra at helium temperature) and the concentration dependent phosphorescence excitation spectra of isotopically mixed crystals the triplet state symmetry and the excitonic Davydov splitting of the low temperature crystalline phase was determined. The resonance pair interaction between the dimer molecules was found to be an order of magnitude smaller than predicted from calculations reported so far.

1. INTRODUCTION

The pyrene crystal is a classical example of an excimer forming crystal. Since its discovery in 1958,[1] the singlet-excimer properties have been studied extensively.[2] Its existence has been attributed to the dimeric arrangement of the molecules in the crystal. For the triplet state, however, various attempts have led to contradictory conclusions:

i) The roomtemperature spectra in delayed fluorescence excitation,[3,4] phosphorescence emission[4] and EPR[5] indicated excitonic triplet states.

ii) Based on phosphorescence emission and lifetime measurements[6,7] in the temperature range between 77 K and 300 K two types of triplet excimers have been postulated, both characterized by a large redshift in the emission spectrum.

The first aim of our work was to solve this discrepancy.

To further elucidate the nature of the triplet state in pyrene new experiments of phosphorescence and delayed fluorescence emission were combined with the photoexcitation method providing the corresponding triplet absorption spectra indirectly.

In our preliminary photoexcitation measurements[8,9] the sensitivity of the triplet spectra on the crystal phase transition at 123 K had turned out, in contrast to the previous findings of no influence on the emission spectra.[6] In the low temperature phase the triplet excitation spectrum decomposes gradually in zerophonon lines and phonon sidebands. The essential features are repeated in Figure 1 for the 0.0–transition of the excitation spectrum. It was intended to verify them in emission as well. Furthermore in the excitation spectrum it had been found out, that the high temperature crystalline phase can be frozen-in under fast cooling conditions. Its spectra at helium temperature gave evidence for a different electron phonon coupling in the triplet state as compared to the low temperature phase.[9] In a further high resolution excitation study of the low temperature spectra a quantitative description within the linear electron phonon coupling could be given.[10]

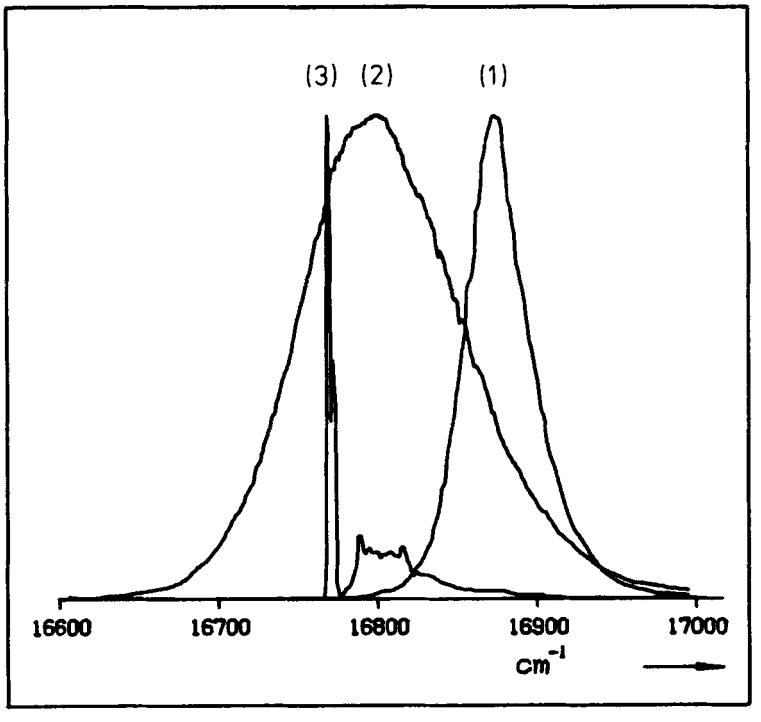

FIGURE 1 0.0 transition of the phosphorescence excitation spectrum at different temperatures: (1) 130 K, (2) 110 K, (3) 2 K.

An additional splitting, however, of the zerophonon line at helium temperature could not be explained yet, but it was argued to correspond to two Davydov components of a triplet excitonic state. In the present work, this interpretation was verified by a detailed polarisation analysis of those lines and their Zeeman patterns. The excitonic triplet state is characterized by intermolecular resonance interactions, which in the low temperature phase are smaller than in the high temperature phase. This has been deduced from photoexcitation spectra of isotopically mixed pyrene crystals.

2. EXPERIMENTAL

The purification of the starting materials, normal pyrene (P-h_{10}) and perdeuterated pyrene (P-d_{10}) was done following a procedure described by Peter and Vaubel.[11] An additional purification with fused potassium was performed. This step obviously removed an impurity causing the sharp decrease of triplet lifetime below 160 K.[11] Zone refining was repeated until a triplet lifetime of 10–60 msec was achieved.

Crystals were grown by the Bridgman method and by sublimation in the vacuum, excluding oxygen. Nonetheless the triplet lifetime in many cases was reduced by a factor of 3 as compared to the value measured before in the zone refining tube. Samples were prepared by cleavage in the *ab*-plane. Thin flakes for the low temperature polarized excitation measurements were prepared by sublimation in a nitrogen atmosphere at 400 mTorr. These flakes could be cooled below the phase transition and warmed up to room temperature without cracking.[12] Examination of the warmed up samples under the microscope revealed no deterioration of the optical quality due to the phase transition, and the extinction between crossed polarizers remained perfect.

The cooling procedure was performed in a Sulfrian variable temperature cryostat. In the region of the phase transition, the cooling rate was kept below 10 K/h. The temperature was measured by calibrated Pt- and Ge-thermistors.

For emission measurements a Coherent Mod. 590 cw-dye laser was used as an excitation source. The output was 0.1–1000 mW in the T_1 region. The spectrometer (0.5 m Bausch and Lomb) was operated at a slit-width corresponding to a resolution of 5–100 cm^{-1}, depending on the intensity of the emission observed. Straylight was avoided by a phosphoroscope (delay time 1–10 msec).

The excitation spectra were taken by scanning the dye laser and recording the integral phosphorescence intensity or delayed fluorescence intensity. The separation of these emissions was achieved by a Schott RG 630 filter,

3 mm thick and a Corning C.S. 5.58, respectively. Stray-light was avoided by crossed choppers or by the filter itself (for delayed fluorescence excitation). The linewidth of the dye laser was 0.001–1.0 cm^{-1} depending on the scanning range, but always 10 times smaller than the reported linewidths.

3. EXPERIMENTAL RESULTS

3.1 Phosphorescence and delayed fluorescence emission of undoped pyrene

Characteristic delayed emission spectra at 170 K are shown in Figure 2. After triplet excitation two types of spectra were observed, Figure 2a and Figure 2b, which led us to distinguish crystal samples of type A and B, respectively.

3.1.1 Crystals of type A The structural features of the spectrum in Figure 2a correspond to the ones previously obtained at 300 K by Peter and Vaubel.[4] The spectrum is dominated by one intense broad band at about 21,000 cm^{-1}. It is the same as observed in the prompt fluorescence containing only singlet excimer emission,[13] and is therefore attributed to delayed excimer fluorescence. In Ref. 4 the structured weak emission of Figure 2a, at the low energy tail of the delayed fluorescence, was attributed to excitonic phosphorescence. Following an increase of the excitation intensity the delayed fluorescence increases stronger than the phosphorescence, the latter becoming obscured by the tail of the former. Making use of this the phosphorescence spectrum could be separated by subtraction of the normalized total spectra in the limits of low and high excitation intensity. In this way the temperature dependence of the excitonic phosphorescence could be demonstrated more clearly, Figure 3. The spectra are not corrected to photoelectrical sensitivity.

Cooling down to 130 K just above the phase transition, a slight monotonic shift of the spectrum to higher energies is observed similar to the excitation spectrum.[9]

When passing the phase transition under slow cooling conditions,[9] a sudden shift of 115 cm^{-1} in the opposite direction is observed. The linewidth slowly decreases between room temperature and phase transition, but then increases abruptly, whereas the structure in the spectrum is maintained independent of the temperature range. Below 110 K the same kind of excitonic phosphorescence is observed only above 40 K, accompanied by a continuous loss of intensity. At low temperatures ($T < 40$ K) another type of phosphorescence appears, further redshifted and gaining intensity with decreasing temperatures, Figure 3c. Higher spectral resolution reveals two series at 2 K with the origin at 16,738 cm^{-1} and 16,724 cm^{-1}, respectively.

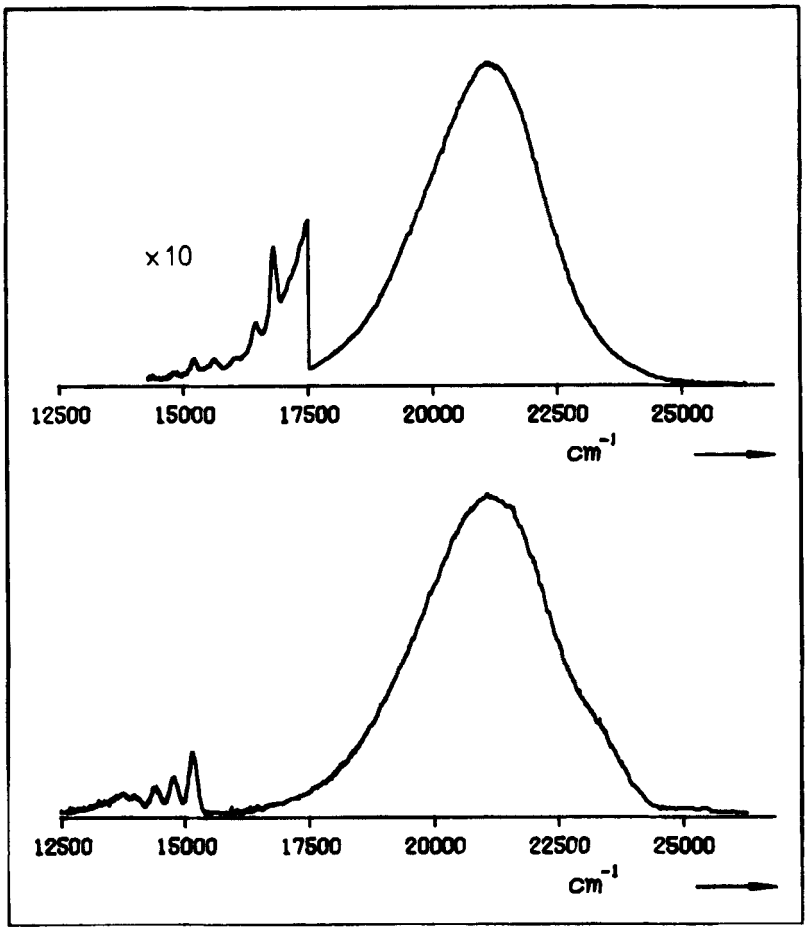

FIGURE 2 Delayed emission spectra of different crystal samples at 170 K: (a) type A (above), (b) type B (below).

The relative intensity of these two series is varying from crystal to crystal. These features allow us to attribute the emission to perturbed pyrene triplet monomers (X-traps).

So far the results of the low temperature (phosphorescence) emission were based on slow cooling conditions[9] through the phase transition, which guarantee the total transformation to the low temperature crystalline phase.

Fast cooling instead, as known from the photoexcitation spectra[9] leads to the freezing in of the high temperature phase at least partially. Excitonic phosphorescence spectra of the frozen-in high temperature phase never have been obtained. But for trap phosphorescence similar to the excitation spectra

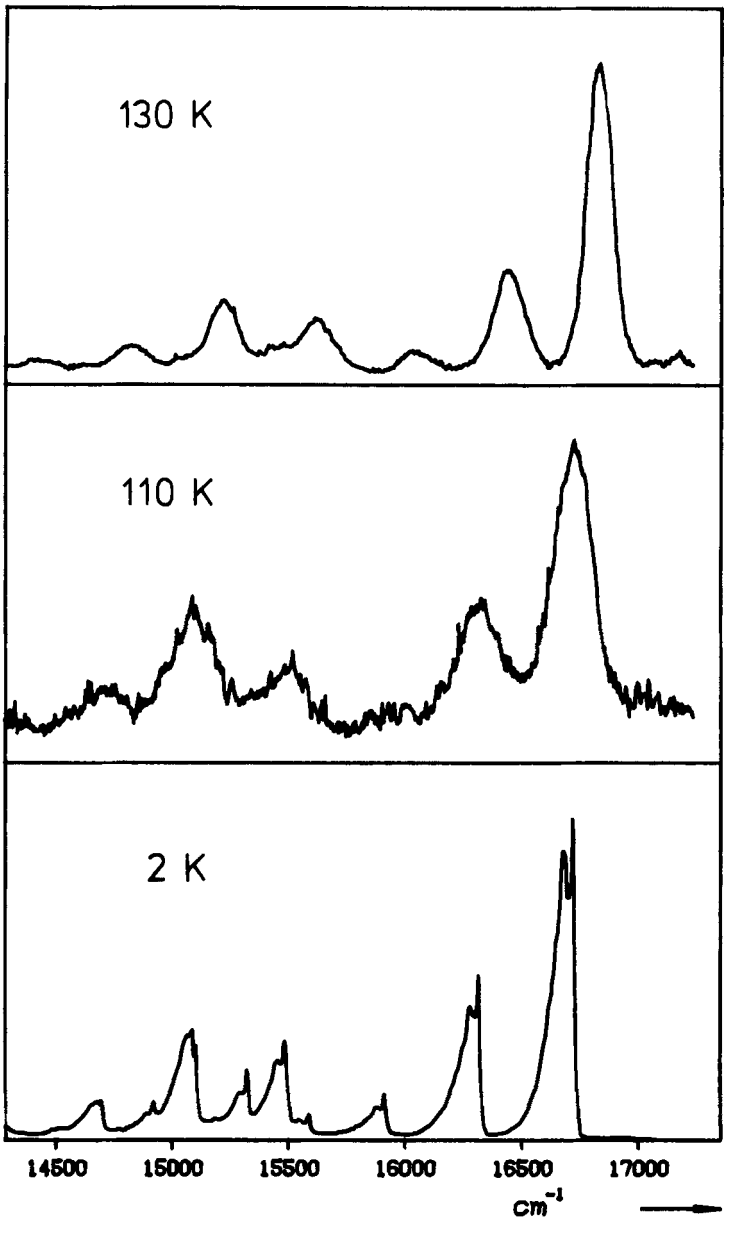

FIGURE 3 Phosphorescence emission of the type A crystal at different temperatures: (a) at 130 K, (b) at 110 K, (c) at 2 K.

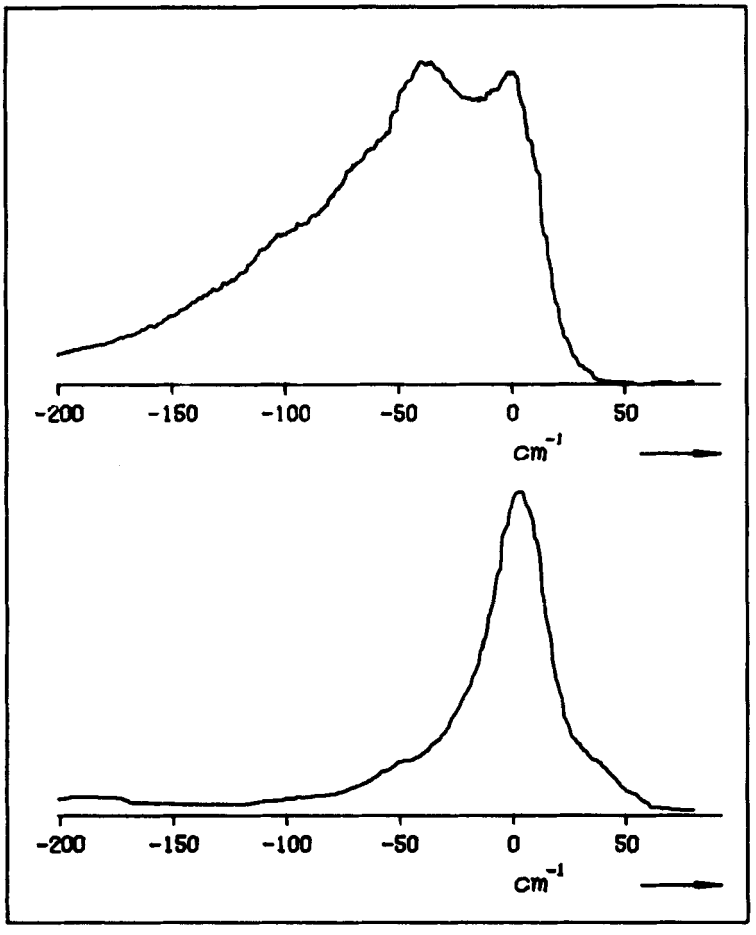

FIGURE 4 0.0 region of the trap emission at helium temperature. Comparison of the low and (frozen-in) high temperature phase. upper and lower curves respectively. In both cases the 0.0 transition was taken as the origin of the energy scale.

it could be demonstrated that the electron-phonon coupling of the triplet state in the frozen-in high temperature phase is distinctly different from that in the low temperature phase and does not show phonon sideband contributions. In Figure 4 the trap phosphorescence of an undoped perdeuterated pyrene (P-d_{10}) crystal is taken as an example for this effect, because a total freezing in is achieved only for P-d_{10}.

3.1.2 Crystals of type B The delayed emission spectrum in Figure 2b differs from that in Figure 2a in two aspects:

i) The delayed fluorescence high energy tail is slightly structured equivalent to the case, in which the prompt fluorescence was found to be modified by monomer contributions.[14]

ii) At the low energy tail an emission appears, which is strongly redshifted compared to the phosphorescence emission in Figure 2a and contains two parts, a structured one consisting of broad bands with a first maximum at 15,200 cm^{-1}, and a structureless one with its maximum at 13,700 cm^{-1} and a total width of 1200 cm^{-1}.

The two parts of the long wavelength emission in Figure 2b correspond to those spectra, which in Ref. 6 had been attributed to a "regular excimer" and to a "defect excimer", respectively. In order to avoid misunderstanding (and not to imply the excimer properties a priori) the following classification will be used: "Regular Phosphoresence" and "Defect Phosphorescence".

Regular phosphorescence (RP) The structured emission was observed between 200 K and 4 K. Lowering the temperature below the phase transition does not result in a change of the vibronic structure, but in a redshift (of about 100 cm^{-1}) similar to the case found for type A crystals (see above). Below 40 K the spectra reveal a substructure, in which narrow lines gain intensity relative to a broadband low energy tail with decreasing temperature, Figure 5b. This behaviour resembles that of X-trap emission, which is present in the B-type crystals, as well, but becomes important relative to the RP-emission only below 4 K. At 4 K under high resolution also two series within the RP-emission are found with origin at 15,164 cm^{-1} and 15,101 cm^{-1}, respectively. Both kinds of emission were measured at higher spectral resolution, from the same crystal, the RP-emission at 4.2 K and the X-emission at 2 K. Figure 6 demonstrates the similar substructure and electron-phonon coupling in the region of spectral origins. But in contrast to the X-spectra the RP-spectra do not show the vibronic substructure due to the pyrene molecule. The prominent vibrational frequencies are 393, 730 and 1114 cm^{-1} (RP), instead of 409, 819 and 1146 cm^{-1} (X). The former frequencies could not be attributed to another molecule.

Defect phosphorescence (DP) The structureless contribution to the spectra was observed in the whole temperature range between 4 K and 300 K. At low temperatures it is superimposed by the RP- and X-phosphorescence. Its behaviour differs in all respects from the other kinds of emissions reported in this work:

i) Its intensity and shape do not depend on temperature (i.e. the phase transiton) significantly.

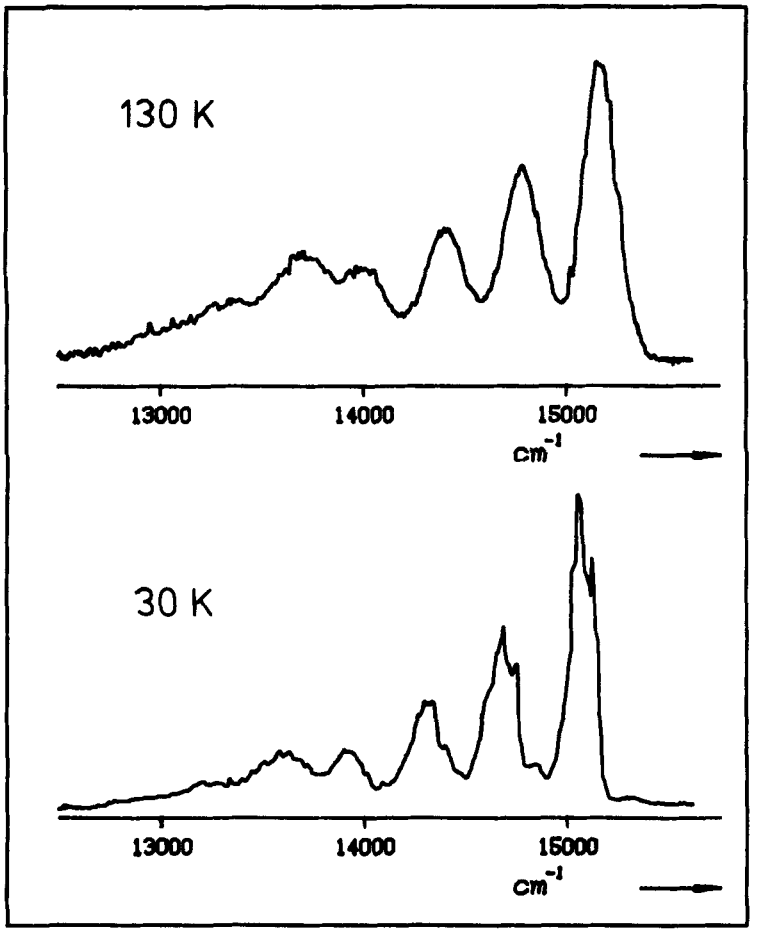

FIGURE 5 Phosphorescence emission of the type B crystal at different temperatures (a) at 130 K, (b) at 30 K.

ii) There is no correlation to the normal triplet excitation spectrum. After excitation in the excitonic 0.0 transition both RP- and DP-emission are measured, at 110 K for instance, Figure 7, lower trace. With the excitation energy reduced by 150 cm^{-1}, however, only the DP-emission is observed, Figure 7, upper trace. Further variation of the excitation wavelength in the spectral region until to 700 nm always gave the same shape of DP-emission, but with the maximum position at constant energy difference of about 3000 cm^{-1} from the excitation.

iii) The DP-emission intensity increases more slowly with increasing excitation intensity than the other emissions and finally saturates.

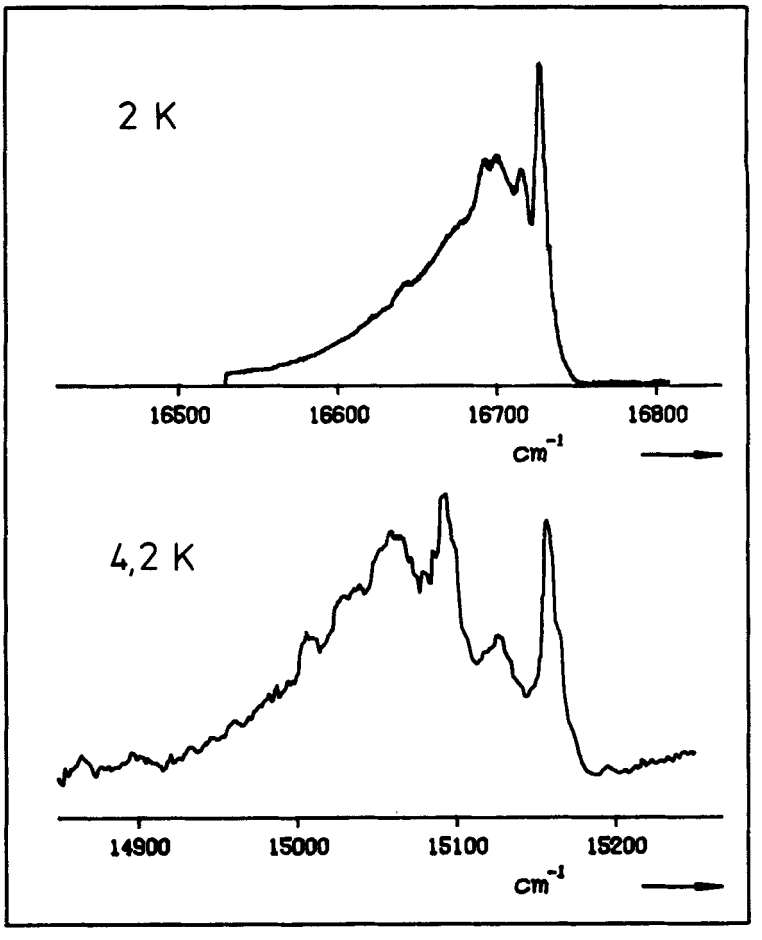

FIGURE 6 Phosphorescence emission of the type B crystal in the helium temperature range. The 0.0 region is given for the X-traps at 2 K (above) and for the RP-traps at 4.2 K (below).

3.2 Further characteristics of crystal types A and B

Besides the spectral differences reported in the preceding sections the following features turned out to be different and characteristic for type A and B crystals, respectively. (The types A and B have to be considered as limiting cases, which are obtained in the vast majority of cases. Actually the intermediate cases also exist.):

i) Triplet lifetimes measured at room temperature reach high values of about 50 msec for type A and are reduced for type B (<20 msec).

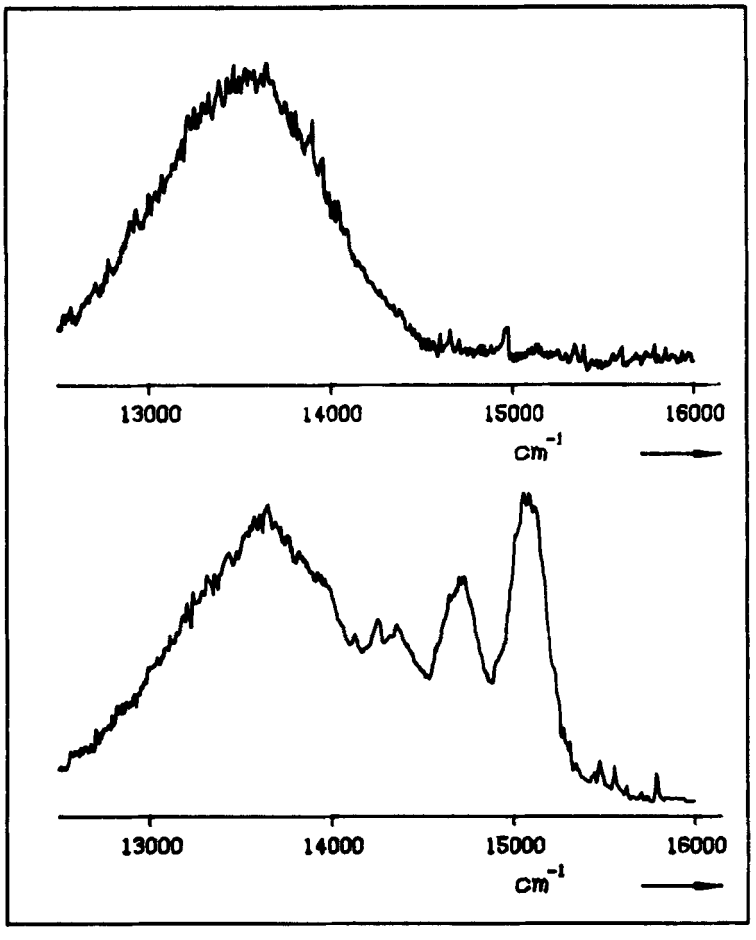

FIGURE 7 Phosphorescence emission of the type B crystal at 110 K after excitation of the 0.0 triplet transition at 16,816 cm^{-1} (below) and 0.0–150 cm^{-1} (above).

ii) The delayed fluorescence intensity is slightly dependent on temperature for type A, but varying orders of magnitude between room temperature and helium temperature for type B, see Figure 8.

iii) The phosphorescence excitation spectra at 4 K are a very sensitive probe for relative trap concentrations in the crystals. Relatively low and high trap concentrations are related to type A and B, respectively.

iv) The absolute Defect Phosphorescence (DP)-emission intensity is correlated to the trap concentration. It is also especially high for thick sublimation crystals.

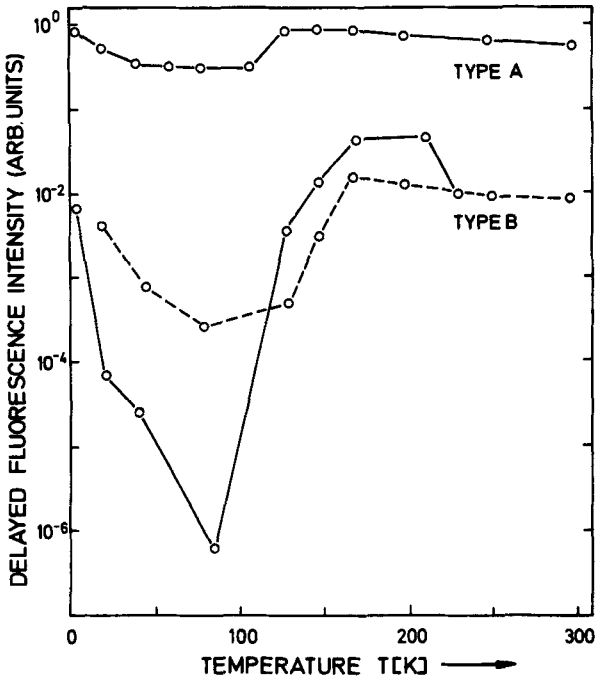

FIGURE 8 Temperature dependence of the delayed fluorescence intensity for crystal types A and B respectively.

3.3 High resolution excitation spectra at 2K

The experimental results to be presented in this section concentrate on the behaviour of the narrow zerophonon lines appearing well separated from the phonon sidebands in the spectra at helium temperature (Figure 1). As discussed already in Ref. 10, thin sublimation crystals of high quality had to be used, in order to allow cooling down through the phase transition without cracking and to reduce the inhomogeneous zerophonon linewidth below their zerophonon splitting ($d = 1.95\ \mathrm{cm}^{-1}$ for the 0.0 transition). Improving the method of handling these crystals the polarization measurements became possible which failed so far.[10] They were limited to the *ab*-crystal plane, however, because the sublimation flakes develop only in this plane. In these excitation spectra there is no distinction between type A and B crystals, respectively.

3.3.1 Polarized spectra of undoped pyrene For high quality crystals a splitting of the zerophonon lines was observed not only for the 0.0 transition, but also for the first two intense vibronic transitions. The splitting decreases

from 1.95 cm^{-1} for the 0.0 to 1.25 cm^{-1} for 0.0 + 409 cm^{-1} and to 0.5 cm^{-1} for the 0.0 + 819 cm^{-1}. The splitting obviously corresponds to the relative intensities of these transitions ($I_0:I_1:I_2$ = 1:0.7:0.3) in accord with the Franck-Condon principle, expected to be valid for the excitonic Davydov components. The possibility that the zerophonon lines belong to different spectral series can be ruled out.

Polarized excitation spectra for the 0.0 components are given in Figure 9 (lower traces). Both components are not uniquely polarized. For the intensity ratios of the upper component (u) and the lower component (1) in excitation

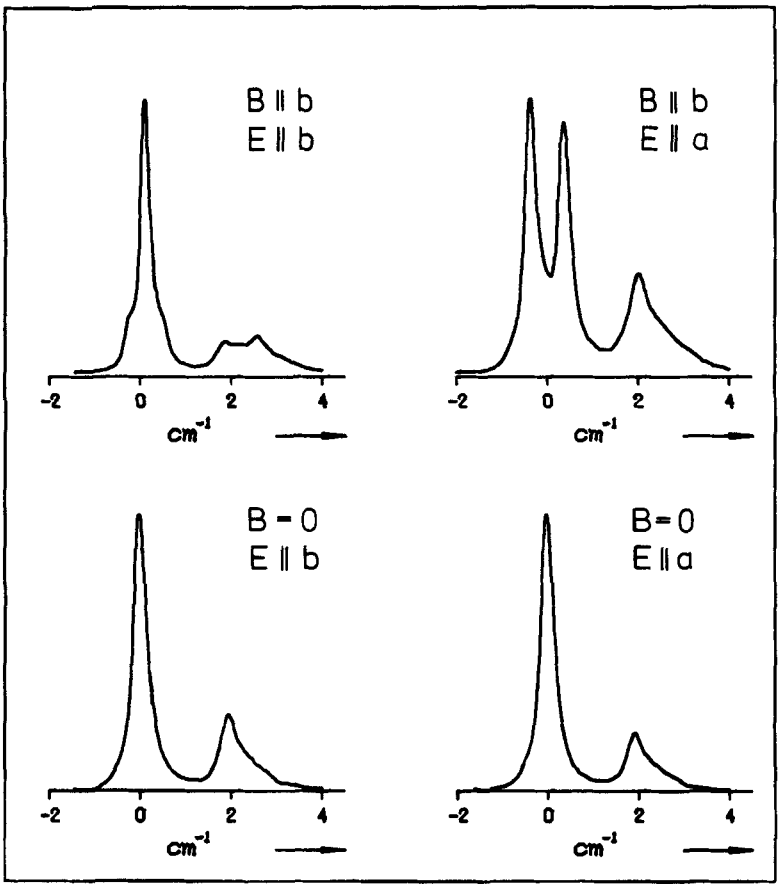

FIGURE 9 Polarized excitation spectra of the 0.0 components at 2 K with and without external magnetic field: $B = 0.4T$, upper traces, and $B \approx 0$, lower traces. (Relative intensities should be compared only within each spectrum.)

$E \| a$ and $E \| b$, respectively, the following values were measured:

$$\left(\frac{I_1}{I_u}\right)_{\| a} = 3.0, \qquad \left(\frac{I_1}{I_u}\right)_{\| b} = 2.5,$$

and for the sum of the intensities $(I_1 + I_u)_{\| a}/(I_1 + I_u)_{\| b} = 1.0$.

The uncertainty is about 10% for the relative and 20% for the absolute values. The results will be discussed later in chapter 4.2.2.

Zeeman spectra of pyrene were investigated for the first time, at magnetic fields of $B = 0.40$ T and with $B \| a$ and $B \| b$. The spectra for $B \| b$ are shown in Figure 9 (upper trace). In the b-polarized spectrum for the lower component the $m = 0$ sublevel is dominant, in that of the upper component the $m = +1$ and $m = -1$ sublevels. For a-polarization the pattern is just reversed for lower and upper components. From these Zeeman spectra the orbital triplet symmetry is deduced: A_u for the lower and B_u for the upper component. Quantitative values will be presented together with the discussion in chapter 4.2.3.

3.3.2 Spectra of perdeuterated pyrene (P-d_{10}) *and mixed crystals of* P-d_{10}: P-h_{10} In the previous reports nothing about the excitation spectra of the perdeuterated analogue of the normal pyrene has been reported. Therefore its main features, which are relevant for this work, will be summarized briefly in the first section.

Undoped P-d_{10}: The properties of the triplet excitation spectra of undoped pyrene P-d_{10} correspond to those of P-h_{10} both in high and low temperature crystalline phase. As the main difference the phase transition occurs at lower temperature ($T = 95$ K). It has been mentioned already above, that the effect of freezing in of the high temperature phase is enhanced in this case and yields a splitting of the 0.0 line $d = 9 \pm 2\,\mathrm{cm}^{-1}$ at 2 K. The vibronic structure reflects the vibronic frequencies of the P-d_{10} molecule.[15] The isotopic shift of the origin in the triplet excitation spectra is $68.5\,\mathrm{cm}^{-1}$ versus higher energy with respect to the undeuterated molecule. At helium temperature the same substructure in the 0.0 region was observed. Whereas the relative intensities of the two zerophonon components are the same as for P-h_{10}, their splitting is slightly reduced ($d = 1.8\,\mathrm{cm}^{-1}$).

P-h_{10} in P-d_{10}: The triplet excitation spectra of isotopically mixed crystals have been investigated as a function of P-h_{10} guest concentration. At helium temperature the spectra contain an additional line, which is redshifted by $67.5\,\mathrm{cm}^{-1}$ as compared to the lower energy 0.0 component of P-d_{10}. Because of its increase in relative intensity proportional to the guest concentration, this line can be attributed to the P-h_{10} "monomer guest" absorption.

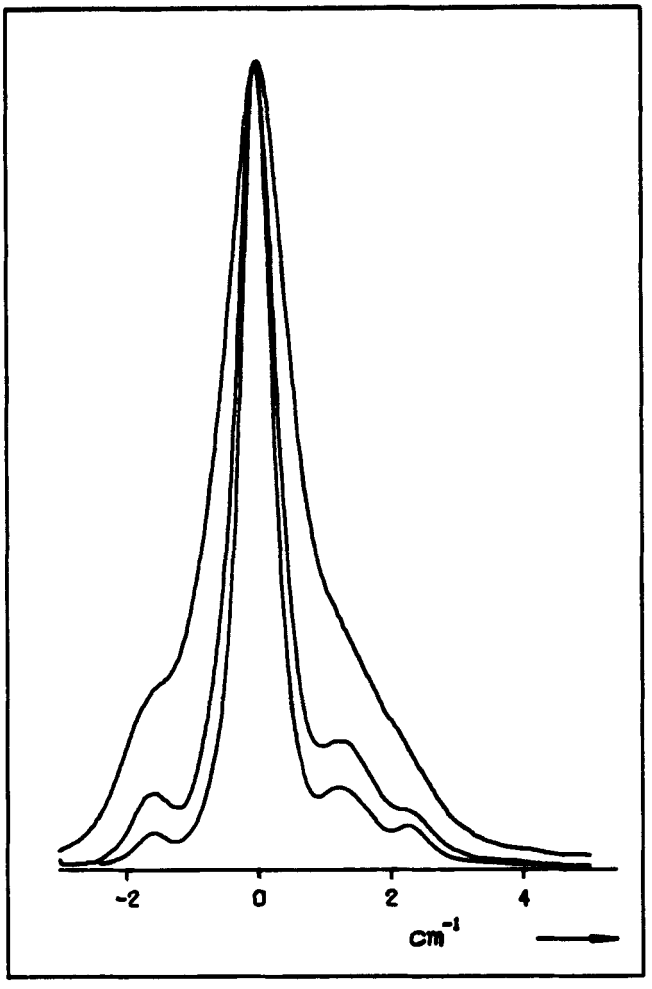

FIGURE 10 Excitation spectra of isotopically mixed crystals P-d_{10}:P-h_{10} at 2 K in the region of the guest origin. Increasing satellite contribution is observed with increasing guest concentration (c_G = 2.4%, 4.3%, 8.0%).

The monomer line itself reveals a substructure at both the low and high energy tail, Figure 10. This substructure is containing concentration dependent and independent contributions. The intensity of the line redshifted by 1.6 cm^{-1} increases linearly relative to the monomer intensity with guest concentration and is therefore unambiguously attributed to a resonance pair. It does not have an equivalent at the high energy side, this was confirmed by computer simulation of the substructure. The existence of at least 3 concentration independent components at the high energy tail is probably due to the

^{13}C substituted monomers, analogous to the readily identified cases of Naphthalene and Anthracene[16] isotopic mixed crystals. Additional observations indicate further pair contributions not resolvable from the monomer line: With increasing guest concentration c_G the linewidth increases rapidly and its position is slightly shifted to the red ($-0.3\,cm^{-1}$ between $c_G = 2.4\%$ and $c_G = 8.0\%$) No further concentration dependent line at greater distance from the monomer has been found, which could belong to the theoretically expected dominating dimeric A_4-interaction (see below).

4. DISCUSSION

4.1 *Triplet exciton versus triplet excimer*

The present experiments clearly demonstrate that the appearance of the excitonic phosphorescence is restricted to crystals of high quality, classified as type A. The general properties of those crystals, specified in chapter 3.2, already made the previous hypothesis very unlikely, that this kind of emission is defect induced[17] and the regular phosphorescence is the genuine triplet emission.[6,7] In the following section a comparative discussion of triplet emission and excitation spectra summarizes further arguments and provides evidence for the excitonic nature of the triplet state. In a second section also the properties of type B crystals are summarized. The spectral features do not allow the attribution to a triplet excimer state.

4.1.1 Temperature dependencies of excitonic phosphorescence and triplet absorption As a reference for this discussion the spectra at 130 K are taken. At this temperature the spectral linewidth is reduced by a factor of three compared to room temperature and provides enough accuracy for the line positions as well. The excitonic phosphorescence spectrum at 130 K exhibits full mirror symmetry to the triplet excitation spectrum with respect to its common origin (which was found at $16{,}873 \pm 15\,cm^{-1}$ in emission in agreement with the absorption value $16{,}876 \pm 5\,cm^{-1}$ reported already in Ref. 9. With increasing temperature both emission and excitation spectra as a whole are shifted to lower energies monotonically, by the same amount between 130 K and 300 K. (For the detailed temperature dependence see Ref. 9).

At temperatures below the phase transition however, the spectral origins are no longer coinciding. The excitonic phosphorescence is redshifted, Figure 2a, by $115 \pm 30\,cm^{-1}$, instead of $60 \pm 15\,cm^{-1}$ in the case of the excitation spectrum.

But this comparison neglects that the maximum position of the broad bands just below the phase transition certainly do not reflect the true origin of the low temperature phase (see Figure 1). Rather it must refer to the average

position of the zerophonon lines in the excitation spectrum at helium temperature. Then the excitonic phosphorescence is found to exhibit the mirror-image of the excitation spectra also in the low temperature crystalline phase within the limits of experimental accuracy.

In conclusion from the mirror symmetry of emission and excitation spectra the excitonic nature of the triplet state has been proven both for the high and low temperature phases.

4.1.2 The so-called triplet excimer emissions From the spectral analysis in chapter 3 the emission of type B crystals clearly could be divided into two parts which had been labelled Regular and Defect Phosphorescence.

The Regular Phosphorescence emission cannot belong to a pyrene triplet excimer because of the following reasons:

i) In the low temperature spectrum a substructure appears with zero phonon lines and phonon sidebands, which resembles the trap phosphorescence very much. The vibronic intervals do not represent pyrene molecular vibrations.

ii) For excimer emission the Stokes shift S and linewidth ΔE should be correlated according to Ref. 18 by $\Delta E = (2kTS)^{1/2}$. In contrast the experiment yields $S = 1600\ \text{cm}^{-1}$, and $\Delta E = 150\ \text{cm}^{-1}$ comparable to the excitonic phosphorescence both at 130 K and 110 K. Also the spectral shift of the origin after phase transition is very similar (about $100\ \text{cm}^{-1}$).

The Defect Phosphorescence emission in the present experiments could not be identified. But evidently it is not related to the pyrene triplet state discussed so far. Whereas the phosphorescence excitation spectrum does not change between excitonic and regular phosphorescence, it is in no respect correlated to the Defect Phosphorescence.

4.2 The triplet excitonic levels of pyrene

4.2.1 Symmetry and energetic position of the Davydov components Both the high[19] and low temperature[20,21] modification of pyrene crystallize in the C_{2h}^5 space group with four molecules in the unit cell. As the molecules occupy general positions within the unit cell, the eigenvalue problem leads to the diagonalization of a complex 4*4 matrix.[22] Neglecting the intermolecular interactions in c-direction and considering only nearest neighbors in the ab-plane (Figure 11), the eigenvalues for $k = 0$ are given by:[22,23]

$$E_{Au,Bu} = E_0 - A_4 \pm 2(A_2 - A_3) \tag{4.1}$$

$$E_{Ag,Bg} = E_0 + A_4 \pm 2(A_2 + A_3) \tag{4.2}$$

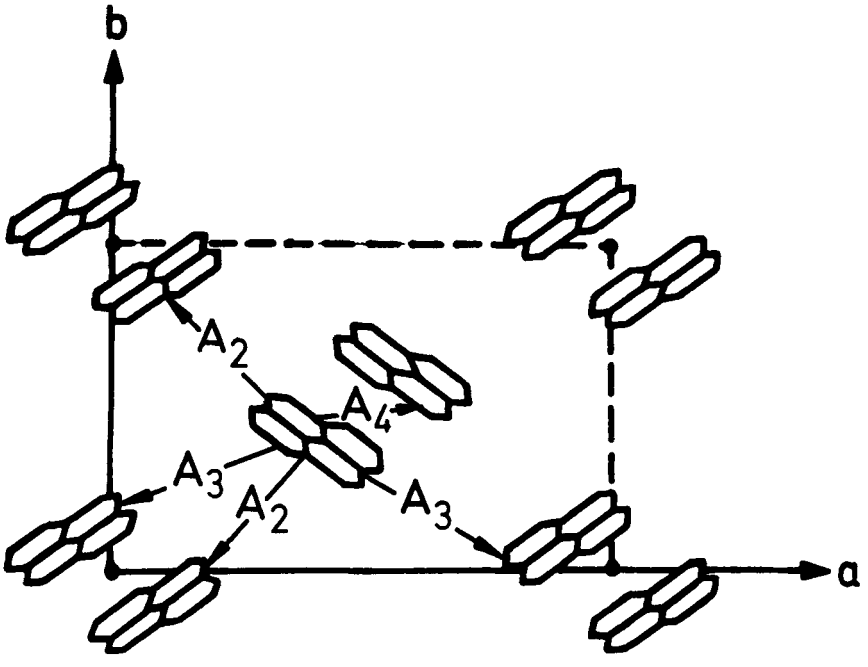

FIGURE 11 Projection of the pyrene crystal onto the *ab*-plane, schematic. Nearest neighbor interactions are labelled A_i.

The A_1 denote the total exchange interactions. E_0 contains the energy of the free molecule, the solvent shift (gas to ideal mixed crystal shift) and the interactions between translationally equivalent molecules. Under the assumption $A_4 > A_2 > A_3 > 0$ the energy levels for the pyrene triplet state are given in Figure 12 schematically.

As only transitions from the A_g ground state to the A_u, B_u are allowed, one should observe a Davydov splitting given by:

$$\Delta = -4(A_2 - A_3) \tag{4.3}$$

In this definition Δ corresponds to the total Davydov splitting of the triplet T_1 state. With the Franck–Condon correction factor for the 0.0 transition, FC $\cong$ 0.25,[3] it describes the observed Davydov splitting. In contrast to crystals of C_{2h}^5 with two molecules per unit cell like naphthalene and anthracene, the measurement of Δ does not give sign and absolute value of one dominating interaction between translationally inequivalent molecules.

The following discussion is concentrated on the low temperature phase, where the mixed crystal spectra provide additional information. For reasons

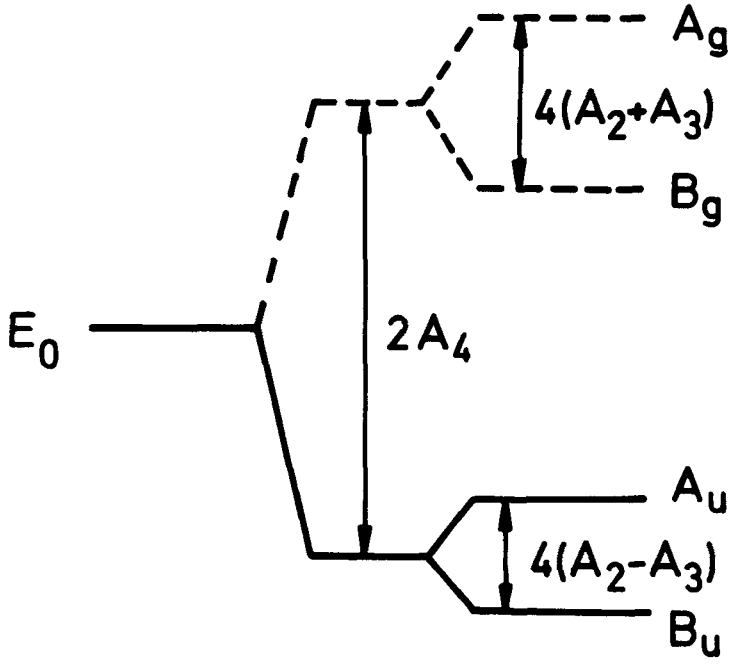

FIGURE 12 Energy levels of the triplet state of pyrene, schematic. The A_i denote the intermolecular exchange interactions within the *ab*-plane (see also Figure 11).

given below the Davydov splitting of the high temperature phase will be discussed separately (Section 4.2.4).

At helium temperature for the low temperature phase the experimental value $\Delta_{0.0} = E_{Bu} - E_{Au} = 1.95\,\mathrm{cm}^{-1}$ was determined (Figure 9, lower traces), with the ordering $E_{Bu} > E_{Au}$ from the Zeeman spectra. This yields $(A_2 - A_3)_{0.0} = -0.5\,\mathrm{cm}^{-1}$. The aim of the measurements on isotopically mixed crystals was to determine the exchange interactions A_i from their individual spectroscopic resonance splittings.

In the present experiments only one resonance pair line has been spectrally resolved, with the indication of additional pair contributions at shorter energetic distances from the monomer guest line (Figure 10). The single pair line must belong to a pair of translationally equivalent neighbors and because of its shift to lower energy ($\Delta E = -1.6\,\mathrm{cm}^{-1}$) to a negative exchange integral.

From all theoretical estimates reported so far[24,25] the largest resonance pair interaction is predicted for A_4, the intra-dimer interaction, and expected to be in the order of $50\,\mathrm{cm}^{-1}$ for the 0.0 contribution. The corresponding large resonance splitting was not observed in the spectra. As shown in the

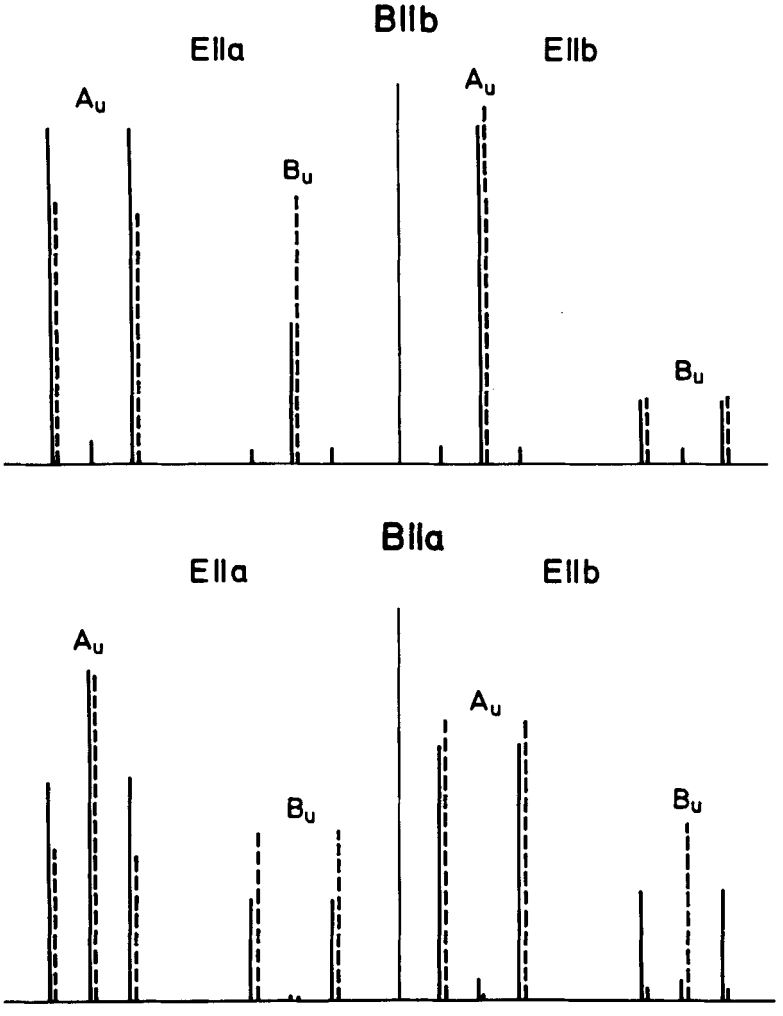

FIGURE 13 Zeeman intensities of the 0.0 Davydov components in polarized light. Comparison of experiment and theory (dashed lines) for the magnetic field directed parallel *a*- and *b*-crystal axis, respectively.

following the experimentally found monomer position provided additional arguments to rule out the possibility for a high A_4 value. The idea was to compare the P-h_{10} monomer energy in the P-d_{10} host with the average energy of the Davydov components of the undoped P-h_{10} crystal.

The monomer guest level E_M was calculated taking into account the interaction with its nearest neighbors only.[26] Treating the problem as two-dimensional and taking into account the interaction of the guest with its 9

nearest host neighbors (Figure 13), numerical diagonalization of the matrix shows the validity of the formula:

$$E_M = \frac{(E_0^d + E_0^h)}{2} \pm \left\{ \left[\frac{(E_0^d - E_0^h)}{2} \right]^2 + A_4^2 \right\}^{1/2} \tag{4.4}$$

where E_0 is defined as above and the upper indices d and h denote the deuterated and the protonated species. In a first approximation the difference $(E_0^d - E_0^h)$ is equivalent to the measured deuteration shift of the Davydov components between undoped P-d_{10} and P-h_{10} crystals ($\Delta E = 68.5\ \mathrm{cm}^{-1}$). For high A_4 values, $A_4 \approx (E_0^d - E_0^h)$, the monomer level should be displaced with respect to the average of the P-h_{10} Davydov components by an amount of about $(E_0^d - E_0^h)/2 \approx 34\ \mathrm{cm}^{-1}$. This is in clear contradiction with the experiment where the monomer energy and the mean value for the Davydov components are identical. Small A_4 values, $A_4 \ll (E_0^d - E_0^h)$ yield $E_M \approx E_0^h$. The monomer is expected to be shifted by an amount of $(A_4)_{0.0}$ from the average position of the P-h_{10} Davydov components. Qualitatively this case describes the experiment much better. From this comparison the possibility of a high A_4 value can be excluded. A medium value should lead to a corresponding pair line in the mixed crystal spectrum at larger distances from the monomer than the only one found experimentally.

Within the limit of a small A_4 the experimental value might be taken into account and tentatively be attributed to the A_4 contribution $(A_4)_{0.0} = -1.6\ \mathrm{cm}^{-1}$. The predicted shift by the same value, however, was not observed experimentally. On the other hand there is a plausible explanation of the residual discrepancy: In the above discussion it had been assumed that the solvent shift contributions included in E_0 are identical for the two cases of the P-h_{10} molecule in the P-d_{10} host and in the P-h_{10} crystal matrix as well. An actual difference of these contributions in the order of $1\ \mathrm{cm}^{-1}$ (which seems to be reasonable[27]) could readily explain the above results.

In conclusion it should be emphasized again, that a small A_4 value must be assumed in order to explain the present experimental results, but contradicts all theoretical estimates reported so far. Qualitatively a large value is expected because of the small interplanar distance of the dimer molecules. A small value, however, could be the result of comparable contributions to A_4 of neutral and charge-transfer interactions with opposite sign.

4.2.2 Polarisation of the Davydov components in zero field Assuming the $T_1 \leftarrow S_0$ transition to gain intensity from the singlet state by spin orbit coupling (SOC), the polarisation of the factor group components depends on the symmetry of the mixing singlet and on the spin orbit route involved.[28] In Table I calculated and experimental values for the polarisation ratios are compared. X-ray data of Rabinovich and Frolov[21] were used for these

TABLE I

Comparison of calculated and experimental polarization ratios of the triplet Davydov Components in zero field

	N-Polarization		Experimental	Mixed Polarization
Spin	L	M	—	$M + N$
Mixing singlet	B_{3u}	B_{3u}	—	$B_{3u} + B_{2u}$
Triplet	B_{2u}	B_{1u}	—	B_{1u}
$\left(\frac{I_{Au}}{I_{Bu}}\right)_{\parallel b}$	0.13	0.99	2.5	2.86
$\left(\frac{I_{Au}}{I_{Bu}}\right)_{\parallel a}$	7.54	1.01	3.0	2.00
$\frac{(I_{Au} + I_{Bu})_{\parallel b}}{(I_{Au} + I_{Bu})_{\parallel a}}$	0.67	0.67	1.0	0.76

calculations. As the phosphorescence was found to be predominantly N (normal to the molecular plane) polarized,[29] the symmetry of the mixing singlet was assumed to be ${}^3B_{3u}$. Neither the assumption of a L (long axis) nor a M (short axis) spin orbit route agrees with the experimental results.

The experimental data are consistent only with a mixed polarization (77% N + 23% M) of the phosphorescence, see the last column of Table I implying the orbital symmetry to be B_{1u}. This finding is in agreement with polarized phosphorescence measurements of pyrene molecules in stretched polyethylene films,[30] explained with 68% N and 32% M transition moment. The residual discrepancy can be explained by assuming a slight change of the pyrene crystal structure between 85 K[21] and 2 K. Variation of the orientation angles as little as one degree is leading already to perfect agreement.

4.2.3 Zeeman spectra The Zeeman patterns for $B \| b$, Figure 9 correspond to the ones calculated from the SOC theory.[28] For $B \| a$ however, experimental and theoretical intensities are clearly different, Figure 11. This discrepancy can be explained by additional processes neglected so far, e.g. crystal field mixing[31] inducing $T_1 \leftarrow S_0$ intensity as well. This process is known to influence rather the intensity ratio between $m = +1$ and $m = 0$ Zeeman lines than the total zero field intensities, and this would explain the experimental findings appropriately.

4.2.4 Davydov splitting in the high temperature phase The detailed knowledge of the spin orbit coupling mechanism allows one to recalculate the factor group splitting in the high temperature phase with greater accuracy. A_u and B_u components are no longer separated due to the large linewidth above the phase transition.[9] Therefore only the value for the oriented gas

ratio was measured:

$$\left(\frac{I_{\|b}}{I_{\|a}}\right)_{\text{total}} = 1.2 \pm 0.12,^{23} \qquad 1.4 \pm 0.3,^{8} \qquad 1.1 \pm 0.1.^{32}$$

The difference d in 0.0 line position is:

$$d = 2.4 \pm 0.6\,\text{cm}^{-1},^{23} \qquad 2.8 \pm 2.0\,\text{cm}^{-1},^{32} \text{ at } 300\text{ K and}$$
$$2.0 \pm 0.3\,\text{cm}^{-1},^{33} \text{ at } 130\text{ K},$$

with the total transition lying at higher energy $\|b$ than $\|a$. The above determined spin orbit route implies a strongly incomplete polarization of the factor group components: $\{(I_{Au}/I_{Bu})_{\|b} = 1.69$, $(I_{Au}/I_{Bu})_{\|a} = 4.87$, using structural data of the high temperature phase.[19] The true value for Δ at 300 K is found to be as large as $\Delta = 5.0\,d \simeq 10\,\text{cm}^{-1}$. The computed value of the oriented gas ratio is $I_{\|b}/I_{\|a} = 1.31$, within the range of experimental values. The calculated Davydov splitting of $10\,\text{cm}^{-1}$ compares well with the splitting of the 0.0 line in the frozen in high temperature phase observed in this work for P-d_{10} at 2 K.

Acknowledgments

The authors are very grateful to Prof. H. C. Wolf for his permanent interest in the progress of this work. They are indebted to the Stuttgarter Kristallabor, in particular to C. Herb, N. Karl, G. Pampel and W. Tuffentsammer, for purification of the starting material and preparation of the various kinds of pyrene crystals used in the present investigations. D. Rabinovich and F. Frolow kindly provided us with X-ray data[21] prior to publication. This work was supported by the Deutsche Forschungsgemeinschaft (SFB 67).

References

1. J. Ferguson, *J. Chem. Phys.*, **28**, 765 (1958).
2. J. B. Birks, editor, Organic Molecular Photophysics, Wiley, London (1975) and references therein.
3. P. Avakian and E. Abramson, *J. Chem. Phys.*, **43**, 821 (1965).
4. L. Peter and G. Vaubel, *Chem. Phys. Lett.*, **21**, 158 (1973).
5. W. Bizzaro, L. Yarmus, J. Rosenthal, and N. F. Berk, *Chem. Phys. Lett.*, **53**, 49 (1978).
6. O. L. J. Gijzeman, J. Langelaar, and J. D. W. van Voorst, *Chem. Phys. Lett.*, **5**, 269 (1970).
7. O. L. J. Gijzeman, W. H. van Leeuwen, J. Langelaar, and J. D. W. van Voorst, *Chem. Phys. Lett.*, **11**, 528 (1971).
8. K. Mistelberger, H. Port, Molecular Spectroscopy of Dense Phases, Proceedings of the 12th European Congress on Molecular Spectroscopy, Elsevier, 181 (1976).
9. H. Port and K. Mistelberger, *J. Luminescence*, **12/13**, 351 (1976).
10. H. Port, K. Mistelberger, and D. Rund, *Mol. Cryst. Liq. Cryst.*, **50**, 11 (1979).
11. L. Peter and G. Vaubel, *Chem. Phys. Lett.*, **18**, 531 (1973).
12. D. Fischer, G. Naundorf, and W. Kloepffer, *Z. Naturforsch.*, **28a**, 973 (1973).
13. J. B. Birks and A. A. Kazzaz, *Proc. Roy. Soc.*, **A304**, 291 (1968).
14. N. J. C. Chu and D. R. Kearns, *Mol. Cryst. Liq. Cryst.*, **16**, 53 (1972).

15. A. Bree, R. A. Kydd, T. N. Misra, and V. V. B. Vilkos, *Spectrochimica Acta*, **27A**, 2315 (1971).
16. H. Port and D. Rund, to be published.
17. O. L. J. Gijzeman, J. Langelaar, and J. D. W. van Voorst, *Chem. Phys. Lett.*, **11**, 526 (1971).
18. M. D. Cohen, E. Klein, Z. Ludmer, and V. Yakhot, *Chem. Phys.*, **5**, 15 (1974).
19. A. C. Hazell, F. K. Larsen, and M. S. Lehmann, *Acta cryst.*, **B28**, 2977 (1972).
20. W. Jones, S. Ramdas, and J. M. Thomas, *Chem. Phys. Lett.*, **54**, 490 (1978).
21. D. Rabinovich and F. Frolow, to be published.
22. V. Ern, *Chem. Phys.*, **25**, 307 (1977).
23. S. Arnold, W. B. Whitten, and A. C. Damask, *Phys. Rev. B*, **3**, 3452 (1971).
24. A. Tiberghien and G. Delacote, *Chem. Phys. Lett.*, **14**, 184 (1972).
25. S. W. Harrison, C. R. Fischer, and S. Arnold, *J. Chem. Phys.*, **57**, 1102 (1972).
26. J. P. Lemaistre, Ph. Pee, R. Lelanne, F. Dupuy, Ph. Kottis, and H. Port, *Chem. Phys.*, **28**, 407 (1978).
27. D. M. Burland and G. Castro, *J. Chem. Phys.*, **50**, 4107 (1969).
28. R. M. Hochstrasser, *J. Chem. Phys.*, **47**, 1015 (1967).
29. R. M. Hochstrasser and S. K. Lower, *J. Chem. Phys.*, **40**, 1041 (1964).
30. J. J. Dekkers, G. Ph. Hoornweg, K. J. Terpstra, C. Maclean, and N. H. Velthorst, *Chem. Phys.*, **34**, 253 (1978).
31. G. Castro and R. M. Hochstrasser, *J. Chem. Phys.*, **48**, 637 (1968).
32. J. L. Fave and M. Schott, *Mol. Cryst. Liq. Cryst.*, **34**, 47 (1976).
33. K. Mistelberger and H. Port, unpublished results.